Progress In Electromagnetics Research, Vol. 105, 365–381, 2010

TRANSIENT RESPONSES OF SOME ANTENNAS UNDER THE IMPACT OF AN INTENTIONALLY INCIDENT HIGH-POWER ELECTROMAGNETIC PULSE

Z. Jiang and W. Y. Yin

Center for Optical and EM Research (COER)
Zhejiang University
Hangzhou 310058, China

Q. F. Liu

Center for Microwave and RF Technologies
Shanghai Jiao Tong University
Shanghai 200240, China

S. Zhang

Center for Optical and EM Research (COER)
Zhejiang University
Hangzhou 310058, China

Abstract—An improved finite difference time domain (FDTD) method is employed for fast capturing transient responses of reconfigurable and multiple-input-multiple-output (MIMO) antennas under the impact of an intentional high-power electromagnetic pulse (EMP) but with different waveforms, respectively, where lumped element and sub-cellular thin-wire algorithms and coaxial feed model are integrated together for handling such three-dimensional antennas used for wireless communication. Parametric studies are carried out to show effects of high-power EMP waveforms, its polarization state and incident direction on the transient coupled voltages on the coaxial feed line and across the diodes, with sufficient information obtained for understanding the interaction between the EMP and the antennas.

Corresponding author: W. Y. Yin (wyyin@sjtu.edu.cn).

1. INTRODUCTION

In the past one decade, significant progress has been made in the development of various advanced antennas used for broadband and multiband multiple-input-multiple-output (MIMO) communication systems [1–3]. Among these, we should to mention reconfigurable antenna [4], MIMO antenna [5], and fractal antenna [6], etc.

On the other hand, it should be understood that electromagnetic environment around us is now becoming more and more complex, because the number of electromagnetic interference (EMI) sources existed is being increased rapidly. Actually, most of communication systems are very sensitive and susceptible to EMI, and in particular to an intentional electromagnetic interference (IEMI) [7–9].

IEMI refers to "intentional malicious generation of electromagnetic energy introducing noise or signals into electrical and electronic systems, thus disrupting, confusing, or damaging these systems for terrorist or criminal purposes" [8, 10]. Such an intentional interfering electromagnetic energy can be generated by a non-explosive high-power microwave source [11], and even a very powerful ultra-wide band pulse antenna [12].

The IEMI usually works in the following way: (a) an intentional high-power or ultra-wide band electromagnetic pulse is suddenly generated and it is incident onto antennas, metallic enclosure with slots, and transmission lines of the communication system through direct radiation or indirect capacitive or inductive coupling; and (b) as a result, it then causes high voltage, large current and rapid temperature rise in the inner circuit which may result in electrical or thermal breakdown and even destruction of the system [13–15].

With respect to IEMI coupling paths with most communication systems, we should at first take radiation coupling between the IEMI and the antenna into account. For a reconfigurable and other MIMO antenna, it usually has active switching feed network or nonlinear device [16, 17]. Under such circumstances, its radiation performance can be easily degraded by an IEMI, and it will be highly challenge to protect it from the attack of an IEMI signal.

Further, we know that the analysis of antenna characteristics in the time domain has been carried out extensively in the past two decades. For example, using finite difference time domain (FDTD) [18–21], we can effectively capture radiation information of various antennas, with the capacity to handle time-varying and nonlinear problems.

In this paper, an improved FDTD method is implemented for investigating transient responses of reconfigurable and MIMO

antennas under the impact of a high-power EMP, respectively. The organization of this paper is arranged as follows. In Section 2, geometries of both reconfigurable and MIMO antennas are presented, and the obliquely incident high-power double-exponential EMP with an arbitrary polarization state is given. In Section 3, an improved FDTD method is outlined, with lumped element and sub-cellular thin-wire algorithms and new coaxial feed model integrated together. In Section 4, numerical calculation is carried out to demonstrate the effects of incident high-power EMP waveform, its polarization state, and its incident direction on the transient coupled voltages on the coaxial feed line and across the diodes of the antennas. Some conclusions are drawn in Section 5.

2. PROBLEM DESCRIPTION

One typical reconfigurable antenna capable of redirecting the main-beam position is proposed in [4]. Figs. 1(a) and (b) show the structure of this pattern-diversity square-ring patch antenna illuminated by an EMP. The square-ring patch with its outer and inner side lengths is set to be 40 and 28 mm [4], respectively. The inside rectangular patch of the dimensions $l \times w$ is etched on the same face of a FR4 printed circuit board, with the thickness of 0.6 mm and the permittivity of 4.4. It is supported by four shorting walls at a height of 7 mm above the ground plane of dimension 100×100 mm^2. The shorting walls A and B have the same width $s = 0.5$ mm, and C and D are connected with ground plane by a pin diode [4], respectively. The gap between the inside

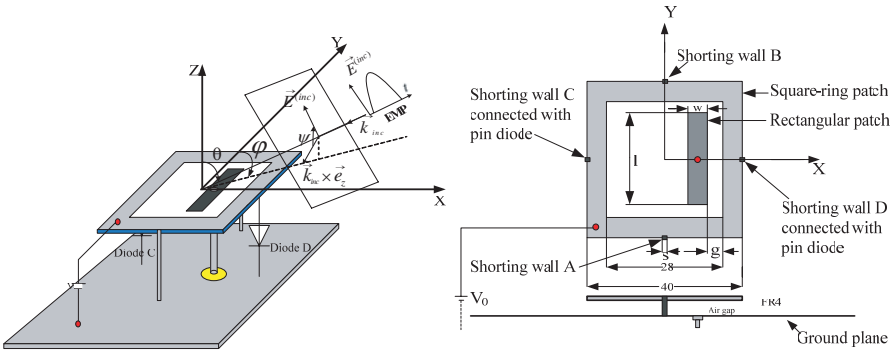

(a) (b)

Figure 1. The geometry of a reconfigurable antenna proposed in [4]. Its (a) 3-D structure; and (b) top view, respectively.

rectangular and the square-ring patches is $g = 9\,\text{mm}$. The antenna is fed by a coaxial line, with its inner radius 0.635 mm and directly connected to the centre of the rectangular patch. Its reconfigurable operation principle can be referred in detail in [4].

On the other hand, we would like to show the geometry of our proposed MIMO antenna, with a high isolation and an extremely closely packed tuneable dual-element planar inverted-F antenna (PIFAs) array [5], as shown in Figs. 2(a)–(c), respectively. It consists of two PIFAs operating at 2.4 GHz for the WLAN with MIMO under the proposed 802.11n standard. Its substrate is made of standard FR4, with the relative permittivity of 4.7 and the thickness of 0.8 mm. The two PIFAs have the length, width and height of $L_{pifa} = 21.6\,\text{mm}$, $W_{pifa} = 6\,\text{mm}$ and $H_{pifa} = 7\,\text{mm}$, respectively. There is a slot cut on the ground plane between two PIFAs, with the width of $d = 1.8\,\text{mm}$, and it plays a critical role in the present mechanism for reducing mutual coupling. A capacitive sheet, with width $W_{cf} = 5\,\text{mm}$, length $l_{cf} = 15\,\text{mm}$ and height $H_{cf} = 3.2\,\text{mm}$, is loaded at the end of the probe [5].

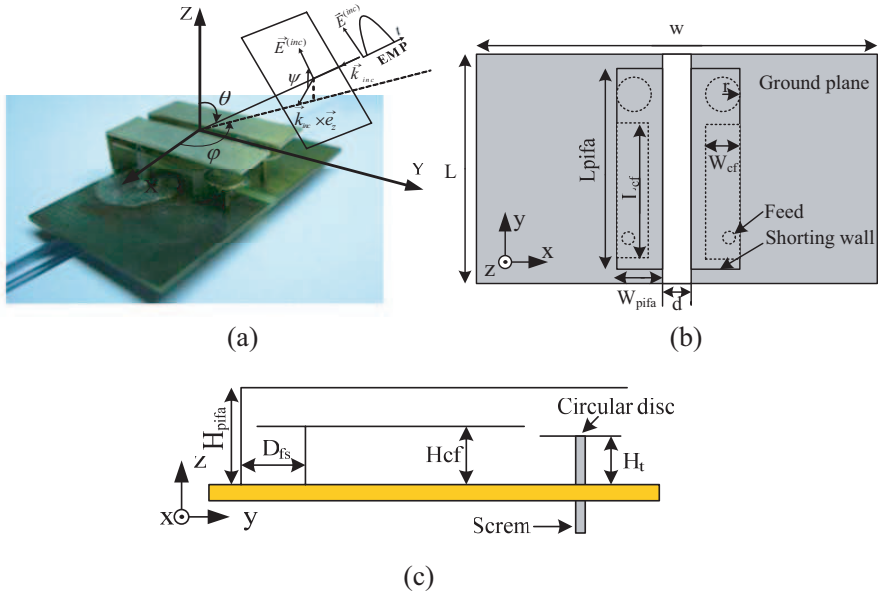

Figure 2. The geometry of a MIMO antenna. Its (a) prototype structure; (b) top view; and (c) cross-sectional view, respectively.

The intentionally incident high-power EMP wave vector in Figs. 1(a) and 2(a) is given by

$$\vec{k}_{inc} = \vec{e}_x \sin\theta\cos\varphi + \vec{e}_y \sin\theta\sin\varphi + \vec{e}_z \cos\theta \tag{1}$$

where $\vec{e}_x, \vec{e}_y$, and $\vec{e}_z$ are three unit vectors in the Cartesian coordinate system; the angles θ and φ are also defined in Fig. 2(a), with $0 < \theta < 180^\circ$ and $0 < \varphi < 360^\circ$. The polarization state of EMP is determined by the polarization angle ψ, and six incident field components are described by

$$E_x^{(inc)} = E^{(inc)}(\sin\varphi\cos\psi - \cos\theta\cos\varphi\sin\psi) \tag{2a}$$

$$E_y^{(inc)} = -E^{(inc)}(\cos\varphi\cos\psi + \sin\varphi\cos\theta\sin\psi) \tag{2b}$$

$$E_z^{(inc)} = E^{(inc)}\sin\varphi\sin\theta \tag{2c}$$

$$H_x^{(inc)} = H^{(inc)}(\sin\varphi\sin\psi + \cos\varphi\cos\theta\cos\psi) \tag{3a}$$

$$H_y^{(inc)} = H^{(inc)}(-\cos\varphi\sin\psi + \sin\varphi\cos\theta\cos\psi) \tag{3b}$$

$$H_z^{(inc)} = -H^{(inc)}\sin\theta\cos\psi \tag{3c}$$

where $E^{(inc)}$, in general, can be described by a double-exponential function as follows:

$$E^{(inc)}(t) = E_0 k(\alpha,\beta)(e^{-\beta t} - e^{-\alpha t}) \tag{4a}$$

and

$$k(\alpha,\beta) = \left(e^{-\beta((\ln(\alpha)-\ln(\beta))/(\alpha-\beta))} - e^{-\alpha((\ln(\alpha)-\ln(\beta))/(\alpha-\beta))}\right)^{-1} \tag{4b}$$

Depending on the values of two parameters α and β [22, 23], the incident high-power EMP can be divided into fast-, medium- and slow-EMP, respectively, as shown in Table 1.

The external pulse in plane wave form will be introduced into FDTD domain using the technique of the total/scattered field [24].

Table 1. The classification of intentionally incident EMP.

Pulse	α (s^{-1})	β (s^{-1})
Fast-EMP	2.0×10^9	7.0×10^6
Medium-EMP	4.8×10^8	2.6×10^6
Slow-EMP	2.0×10^8	1.0×10^6

3. IMPROVED FDTD METHOD

With respect to the above three-dimensional structures in Figs. 1 and 2, traditional FDTD is not able to handle thin wire, lumped element, and coaxial feed probe enclosed. Therefore, an improved FDTD method will be proposed for the analysis of their transient responses.

3.1. Lumped Element and Thin-wire Sub-cellular Algorithm

As we apply the Maxwell's curl equation to the lumped element in the FDTD domain in Figs. 1(a) and (b), we have

$$\nabla \times \vec{H} = \vec{J}_C + \frac{\partial \vec{D}}{\partial t} + \vec{J}_L \tag{5}$$

where $\vec{J}_C = \sigma \vec{E}$, $\vec{D} = \varepsilon \vec{E}$, and the local current density of the lumped element is related to the total current I_L by $J_L = I_L/(\Delta x \Delta y)$. Then, (5) can be turned into [24]

$$\begin{aligned} E_z^{n+1}(i,j,k+1/2) = {} & E_z^n(i,j,k+1/2) + \Delta t \cdot (\nabla \times H)_z^{n+1/2}(i,j,k+1/2)/\varepsilon_0 \\ & - \Delta t \cdot I_L^{n+1/2}(i,j,k+1/2)/(\varepsilon_0 \Delta x \Delta y) \end{aligned} \tag{6}$$

For the lumped element of z-directed resistor R located in the free space at the field component E_z, we have

$$\begin{aligned} I_{ZL}^{n+1/2}(i,j,k+1/2) &= \Delta z E_z^{n+1/2}(i,j,k+1/2)/R \\ &= \Delta z [E_z^{n+1}(i,j,k+1/2) + E_z^n(i,j,k+1/2)]/(2R) \end{aligned} \tag{7}$$

Substituting (9) into (6), we obtain

$$\begin{aligned} E_z^{n+1}(i,j,k+1/2) = {} & \left[\left(1 - \frac{\Delta t \Delta z}{2R\varepsilon_0 \Delta x \Delta y} \right) E_z^n(i,j,k+1/2) \right. \\ & \left. + (\Delta t/\varepsilon_0) \times (\nabla \times H)_z \Big|_{i,j,k+1/2}^{n+1/2} \right] \Big/ \left(1 + \frac{\Delta t \Delta z}{2R\varepsilon_0 \Delta x \Delta y} \right) \end{aligned} \tag{8}$$

As for the lumped element of a capacitor C located in the free space at E_z, we obtain [24]

$$\begin{aligned} I_{ZL}^{n+1/2}(i,j,k+1/2) &= C \frac{d}{dt} \Delta z E_z^{n+1/2}(i,j,k+1/2) \\ &= C \Delta z [E_z^{n+1}(i,j,k+1/2) - E_z^n(i,j,k+1/2)]/\Delta t \end{aligned} \tag{9}$$

Also, substituting (7) into (6), we get

$$\begin{aligned} E_z^{n+1}(i,j,k+1/2) = {} & E_z^n(i,j,k+1/2) + (\Delta t/\varepsilon_0) \times [1 + C\Delta z/(\Delta x \Delta y)] \\ & \times (\nabla \times H)_z^{n+1/2}(i,j,k+1/2) \end{aligned} \tag{10}$$

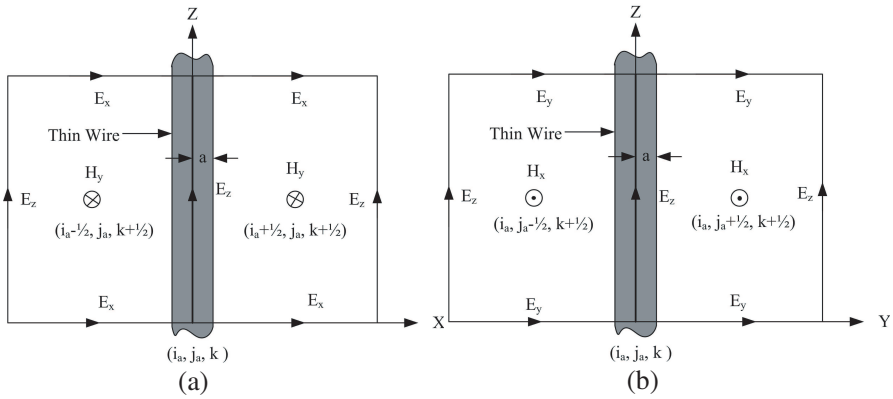

Figure 3. Faraday's law contour path for the thin wire in Fig. 1(a) at the x-z plane; (b) at the y-z plane.

We have several choices to simulate thin wire probe feed in FDTD domain in Figs. 1 and 2. In [25], both adjacent electric and magnetic fields are corrected according to the wire radius, the field correction is carried out by modifying both equivalent permittivity and permeability of the adjacent cells. The other choice is to use a set of standard thin-wire FDTD equations proposed in [26]. As the feed is a coaxial line, the later will be implemented in our FDTD algorithm, Fig. 3 illustrates the geometry used for driving special FDTD time-stepping expression for the circumferential looping H- and radial E-component immediately adjacent to a z-aligned thin wire.

As an example, for the looping H_y-component, we have

$$H_y^{n+1/2}(i_a+1/2, j_a, k+1/2) = H_y^{n-1/2}(i_a+1/2, j_a, k+1/2) - (\Delta t/(\mu_0 \Delta z))[E_x^n(i_a+1/2, j_a, k+1) - E_x^n(i_a+1/2, j_a, k)] + (\Delta t/(\mu_0 \Delta x))(2/\ln(\Delta x/a))E_z^n(i_a+1, j_a, k+1/2) \quad (11a)$$

$$H_x^{n+1/2}(i_a, j_a+1/2, k+1/2) = H_x^{n-1/2}(i_a, j_a+1/2, k+1/2) - (\Delta t/(\mu_0 \Delta z))\,[E_y^n(i_a, j_a+1/2, k+1) - E_y^n(i_a, j_a+1/2, k)] + (\Delta t/(\mu_0 \Delta y))(2/\ln(\Delta x/a))\,E_z^n(i_a, j_a+1, k+1/2) \quad (11b)$$

where $a = 0.2\,\text{mm}$.

3.2. Equivalent Coaxial Line Feed Model

More recently, an equivalent feed model for the FDTD analysis of an antenna excited by a coaxial line is proposed [27]. Here, we further modify its mathematical equations which are applicable for the Cartesian coordinate system. Using the quasi-static approximation,

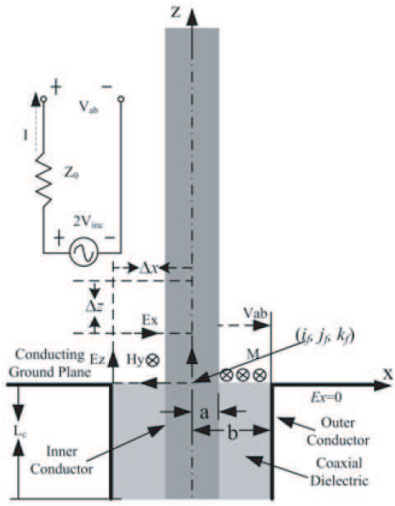

Figure 4. The equivalent magnetic-frill current and the equivalent load circuit of a cylindrical monopole antenna fed by a coaxial line [28].

the coaxial aperture is represented as an equivalent magnetic-frill current, as show in Fig. 4. According to the theory of transmission line [28], the total voltage at the aperture with the load terminal of the line should be equal to the superposition of the incident $V_{inc}(t)$ and the reflected one denoted by $V_{ref}(t)$, i.e.,

$$V_{ab}(t) = V_{inc}(t) + V_{ref}(t) \tag{12}$$

For a lossless line with a characteristic impedance Z_0, the reflected voltage

$$V_{ref}(t) = V_{inc}(t) - Z_0 I \tag{13}$$

The equivalent magnetic-frill current, including the effects of TEM mode, is described by

$$M(x, y, t) = [-2V_{inc}(t) + Z_0 \cdot I(t)]/[a \ln(b/a)] \tag{14}$$

where $b = 0.5\,\text{mm}$ assumed.

According to the Ampere's law, the feed current $I(t)$ can be calculated by

$$\begin{aligned} I(t=n\Delta t) \equiv I^n = \Delta y \left[H_y^n(i_f + 1/2, j_f, k_f) - H_y^n(i_f - 1/2, j_f, k_f)\right] \\ -\Delta x \left[H_x^n(i_f, j_f + 1/2, k_f) - H_x^n(i_f, j_f - 1/2, k_f)\right] \end{aligned} \tag{15}$$

where i_f, j_f and k_f are the spatial grid points of the feed cell, and the discrete time $t = nt$. According to the thin-wire approximation

given in [26], as to the feed cell, Equations (13a) and (13b) will be changed, (14) and (18) are further applied for the feed cell, and the update equation of the magnetic field is expressed as

$$\begin{aligned} &H_y^{n+1/2}(i_f+1/2, j_f, k_f) = H_y^{n-1/2}(i_f+1/2, j_f, k_f) \\ &-(\Delta t/(\mu_0 \Delta z))\ E_x^n(i_f+1/2, j_f, k_f) \\ &+(\Delta t/(\mu_0 \Delta x))(2/\ln(\Delta x/a))\ E_z^n(i_f+1, j_f, k_f) \\ &-(\Delta t/(\mu_0 \Delta z))(2/\ln(\Delta x/a))(-2V_{inc}^n + Z_0 \cdot I^n)/\Delta x \end{aligned} \tag{16}$$

$$\begin{aligned} &H_x^{n+1/2}(i_f, j_f+1/2, k_f) = H_x^{n-1/2}(i_f, j_f+1/2, k_f) \\ &+(\Delta t/(\mu_0 \Delta z))E_y^n(i_f, j_f+1/2, k_f) \\ &-(\Delta t/(\mu_0 \Delta y))\ (2/\ln(\Delta y/a))\ E_z^n(i_f, j_f+1, k_f) \\ &+(\Delta t/(\mu_0 \Delta z))(2/\ln(\Delta y/a))(-2V_{inc}^n + Z_0 \cdot I^n)/\Delta y \end{aligned} \tag{17}$$

The reflected feed voltage is obtained by

$$V_{ref}^n = V_{inc}^n - Z_0 \cdot I^n \tag{18}$$

4. NUMERICAL RESULTS AND DISCUSSION

To verify our developed improved FDTD algorithm, Figs. 5(a) and (b) show the calculated return losses of the above reconfigurable and MIMO antennas, respectively, but with no intentional EMP introduced. The computational domain is discretized with cubic cells of $\Delta x = \Delta y = 0.5\,\text{mm}$, $\Delta z = 0.2\,\text{mm}$, the time step is $\Delta t = \Delta z/(2c_0)$, $c_0 = 3 \times 10^8\,\text{m/s}$; and 20 layers of perfectly matching layer (PML) absorbing boundary is employed to truncate the computational domain. The return losses are calculated by [29]. As for the diode, we make use of two equivalent circuit models to deal with its ON- and OFF-state, respectively, i.e., when the pin switch diode is in the ON-state, its equivalent circuit just includes a resistor about $0.9\,\Omega$. When it is in the OFF-state, the diode can be equivalent to a capacitor about 0.2 pF [4]. In Fig. 5(a), the return losses corresponding to both ON- and OFF-state of two pin diodes are considered, and good agreements are obtained with those of the measured results given in [4]. In Fig. 5(b), excellent agreements are also obtained between our FDTD algorithm and that of commercial software HFSS for the MIMO antenna.

Further, Fig. 6 shows the calculated radiation patterns of the reconfigurable antenna using our hybrid FDTD algorithm on the y-z plane at 2.16 GHz, with both diodes set at OFF-state. It is further indicated that our algorithm is able to predict the radiation characteristics of the above antenna accurately.

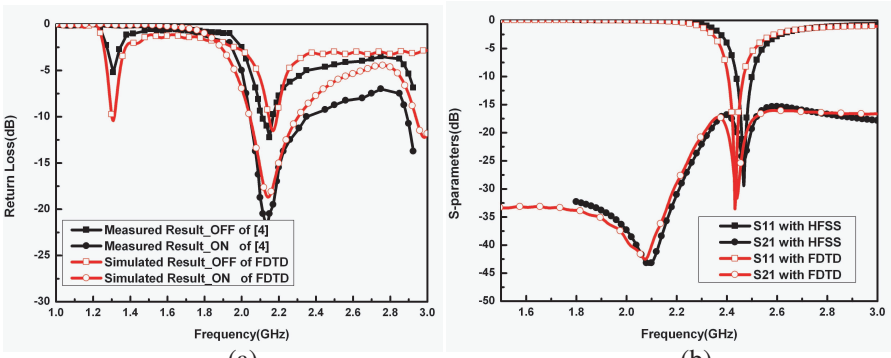

(a) (b)

Figure 5. Comparison of the calculated return losses obtained by our hybrid FDTD algorithm, measurement, and commercial software HFSS, respectively. (a) Reconfigurable; and (b) MIMO antennas, respectively.

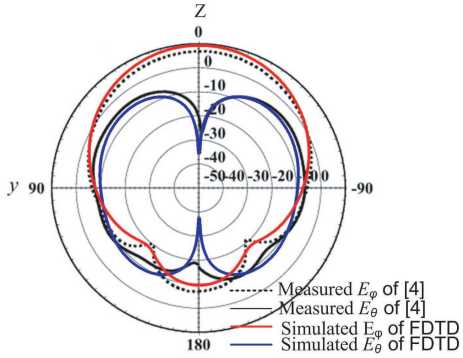

Figure 6. Comparison of the calculated radiation pattern on the y-z plane using our improved FDTD algorithm and that of measurement, with both diodes set at OFF-state.

Now, we examine the transient voltage responses on the coaxial line of the above reconfigurable antenna illuminated by a high-power fast-, medium-, and slow-EMP of $E_0 = 50\,\mathrm{kV/m}$, respectively, but with the same incident direction of $\varphi = \theta = 0^\circ$ and polarization angle of $\psi = 0^\circ$ assumed. Two diodes are also set at OFF-state. It is shown that among three types of intentional high-power EMP incidence, the fast-EMP excites the strongest coupled voltage on the coaxial feed line of the reconfigurable antenna.

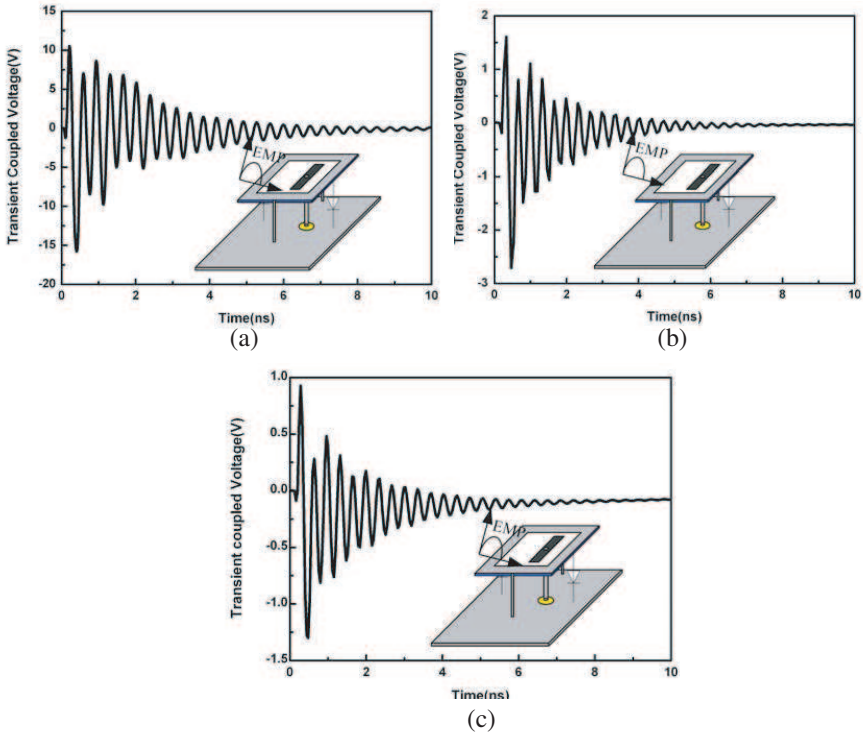

Figure 7. The transient voltage responses on the coaxial feed line of the reconfigurable antenna illuminated by a high-power (a) fast-EMP; (b) medium-EMP; and (c) slow-EMP, respectively.

Figure 8 shows the transient voltage response on the coaxial line of MIMO antenna in Fig. 2, which is also illuminated by a high-power fast-, medium- and slow-EMP, respectively, with the same incident direction and polarization angle as assumed in Fig. 7. Evidently, the transient coupled voltage excited by the fast-EMP is also the strongest among three EMP incidences.

We further examine the effects of the incident fast-EMP polarization angle on the transient voltage response of the antenna, where $\psi = 30°$, $90°$, and $150°$, respectively, but the incident EMP direction is kept to be $\varphi = \theta = 90°$. It is shown that the transient coupled voltages on the coaxial feed line and across the diode C are very sensitive to the variation of ψ. In particular, when $\psi = 90°$, the transient coupled voltage reaches its lowest level among three cases. Fortunately, the maximum in Fig. 9(b) is still smaller than the switch voltage 1.5 V of the diode. However, as the magnitude of the incident

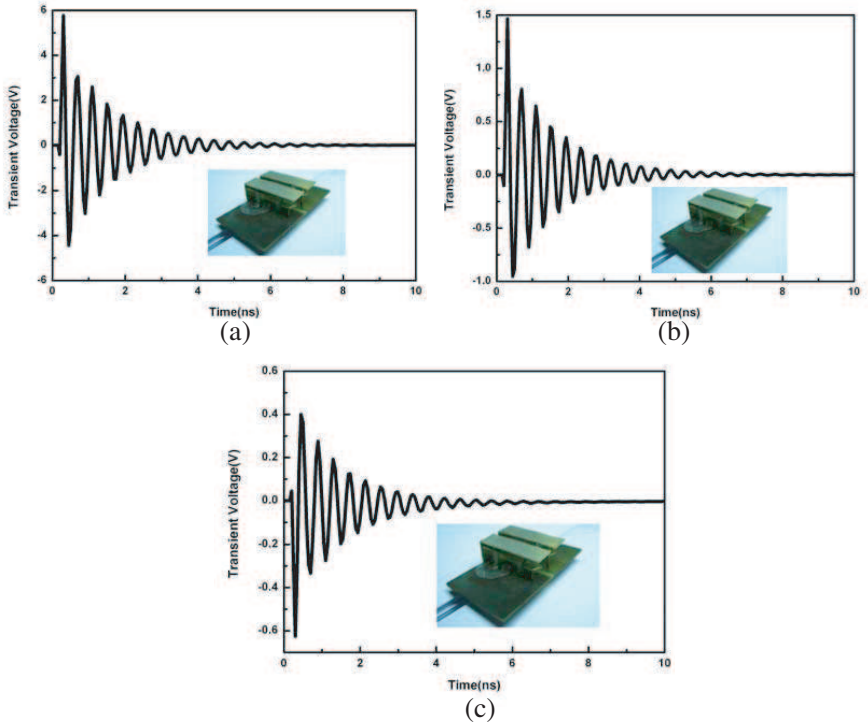

Figure 8. The transient voltage responses on the coaxial feed line of the MIMO antenna illuminated by a high-power (a) fast-EMP; (b) medium-EMP; and (c) slow-EMP; respectively.

high-power EMP further increases, it will cause its switching problem. On the other hand, it should be understood that, as the coupled voltage ($\psi = 30^\circ$ or 150°) is transmitted into the inner circuit of the system through the coaxial feed line, it is able to cause electro-thermal breakdown of most active MOS devices.

Figure 10 shows the transient coupled voltages on the coaxial feed line of the reconfigurable antenna for $\theta = 45^\circ$ and $\psi = 90^\circ$, but $\varphi = 45^\circ, 90^\circ$ and 135°, respectively. It is observed that the voltage waveforms have little difference among three cases. This is because the radiation patterns at $\phi = 45^\circ$, 90° and 135° are approximately the same as plotted in [4].

We now change the incident EMP direction from $\theta = 45^\circ$, 90° to 135°, respectively, but with $\phi = 60^\circ$ and $\psi = 90^\circ$. Correspondingly, the coupled voltages on the coaxial feed line and across the diode C of the reconfigurable antenna are plotted in Fig. 11. It is evident that

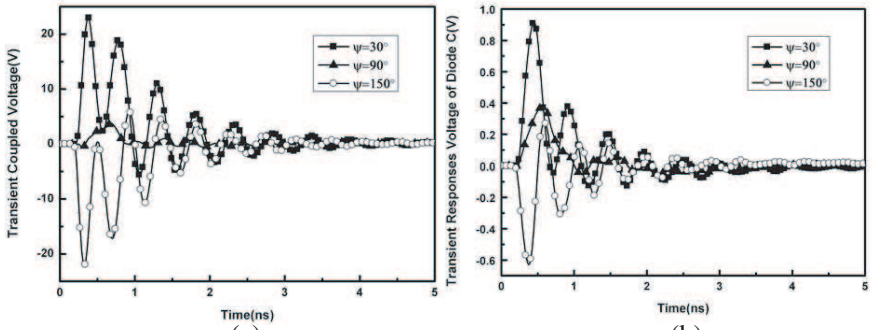

(a) (b)

Figure 9. The transient coupled voltages (a) on the coaxial feed line; and (b) across the diode C of the reconfigurable antenna illuminated by a high-power fast-EMP but for different polarization angles.

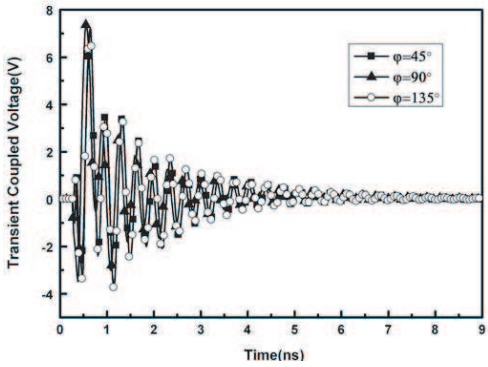

Figure 10. The transient coupled voltage on the coaxial feed line of the reconfigurable antenna illuminated by a high-power fast-EMP for different values of $\phi = 45°$, $90°$ and $135°$, but with $\theta = 45°$ and $\psi = 90°$.

when $\theta = 45°$ the coupled voltage is much larger than that of $\theta = 90°$, as shown in Fig. 11(a). This can be understood that the antenna gain at $\theta = 45°$, as plotted in [4], is the largest among the three cases here. Also, it is observed that the coupled voltage across the diodes in Fig. 11(b) is the lowest.

As the incident EMP is as high as $E_0 = 70\,\text{kV/m}$, the coupled voltage across both diodes exceeds the switch voltage 1.5 V, and this imply that their switching state is disturbed by the high-power EMP. Under such condition, such a reconfigurable antenna cannot be operated properly.

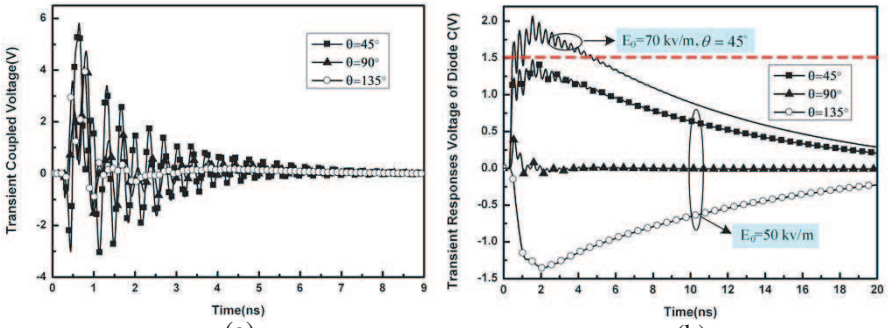

Figure 11. The transient coupled voltages (a) on the coaxial feed line; and (b) across the diodes of the reconfigurable antenna illuminated by a high-power fast-EMP for different values of θ, but with $\phi = 60°$ and $\psi = 90°$.

5. CONCLUSIONS

In this paper, the transient responses of reconfigurable and MIMO antennas under the impact of intentional high-power electromagnetic pulse are investigated using an improved FDTD method, with lumped element and sub-cellular thin-wire algorithm and new coaxial feed model integrated together. Numerical results are presented to show the effects of different pulse waveform parameters on the transient coupled voltages on the coaxial feed line and across the diodes of the antennas, also including the incident EMP direction and polarization state, etc. Therefore, the above study can provide us sufficient information about the interaction of an intentional high-power EMP with the above antennas, which is essential for protecting circuits inside the communication system from the attack of an IEMI.

ACKNOWLEDGMENT

The authors appreciate the financial support of the State Key Lab of MOI, Department of Optical Engineering of Zhejiang University of China. Wen-Yan Yin and Q. F. Liu also appreciated the financial support of the NSF under Grant of 60831002 of China.

REFERENCES

1. Jafargholi, A. and M. Kamyab, "Pattern optimization in an UWB spiral array antenna," *Progress In Electromagnetics Research M*, Vol. 11, 137–151, 2010.
2. Vazquez Antuna, C., G. Hotopan, S. Ver Hoeye, M. Fernandez Garcia, L. F. Herran Ontanon, and F. Las-Heras, "Microstrip antenna design based on stacked patches for reconfigurable two dimensional planar array topologies," *Progress In Electromagnetics Research*, Vol. 97, 95–104, 2009.
3. Ghassemi, N., J. Rashed-Mohassel, M. H. Neshati, and M. Ghassemi, "Slot coupled microstrip antenna for ultra wideband applications in C and X bands," *Progress In Electromagnetics Research M*, Vol. 3, 15–25, 2008.
4. Chen, S. H., J. S. Row, and K. L. Wong, "Reconfigurable square-ring patch antenna with pattern diversity," *IEEE Trans. Antennas Propagat.,* Vol. 55, No. 2, 472–475, Feb. 2007.
5. Zhang, S., S. N. Khan, and S. He, "Reducing mutual coupling for an extremely closely-packed tunable dual-element PIFA array through a resonant slot antenna formed in-between," *IEEE Trans. Antennas and Propagation*, April 2010 (accepted).
6. Gianvittorio, J. P. and Y. Rahmat-Samii, "Fractal antennas: A novel antenna miniaturization technique, and applications," *IEEE Trans. Antennas Propag. Mag.,* Vol. 44, No. 1, 20–36, Feb. 2002.
7. Radasky, W. A., C. E. Baum, and M. W. Wik, "Introduction to the special issue on high-power electromagnetics (HPEM) and intentional electromagnetic interference (IEMI)," *IEEE Trans. Electromagn. Compat.,* Vol. 46, No. 3, 314–321, Aug. 2004.
8. Giri, D. V. and F. M. Tesche, "Classification of intentional electromagnetic environments (IEME)," *IEEE Trans. Electromagn. Compat.,* Vol. 46, No. 3, 322–328, Aug. 2004.
9. "Revision of Part 15 of the commission's rules regarding ultra-wideband transmission systems," *Tech. Rep., ET-Docket*, 98–153, FCC02-48, Federal Communications Commission, 2002.
10. Xue, M. F. and W. Y. Yin, "Wide band pulse responses of fractal monopole antennas under the imapct of an EMP," *IEEE Trans. Electromagn. Compat.,* Vol. 52, No. 1, 98–107, Feb. 2009.
11. Sabath, F., M. Backstrom, B. Nordstrom, D. Serafin, A. Kaiser, B. A. Kerr, and D. Nitsch, "Overview of four European high-power microwave narrow-band test facilities," *IEEE Trans. Electromagn. Compat.*, Vol. 46, No. 3, 329–334, Aug. 2004.
12. Prather, W. D., C. E. Baum, R. J. Torres, F. Sabath,

and D. Nitsch, "Survey of worldwide high-power wideband capabilities," *IEEE Trans. Electromagn. Compat.,* Vol. 46, No. 3, 335–344, Aug. 2004.

13. Xu, J. F., W. Y. Yin, and J. F. Mao, "Transient thermal analysis of GaN heterojunction transistors for high-power applications," *IEEE Microwave and Wireless Components Lett.*, Vol. 17, No. 1, 55-57, Jan. 2007.
14. Xu, J. F., W. Y. Yin, J. F. Mao, and L. W. Li, "Thermal transient response of GaAs FETs under intentional electromagnetic interference (IEMI)," *IEEE Trans. Electromagn. Compat.*, Vol. 50, No. 2, 340–346, May 2008.
15. Ren, Z., W.-Y. Yin, Y.-B. Shi, and Q. H. Liu, "Thermal accumulation effects on the transient temperature responses in LDMOSFETs under the impact of a periodic electromagnetic pulse (EMP)," *IEEE Trans. Electron Devices*, Vol. 57, No. 1, 345–352, Jan. 2010.
16. Nikolaou, S., R. Bairavasubramanian, C. Lugo, I. Carrasquillo, D. C. Thompson, G. E. Ponchak, J. Papapolymerou, and M. M. Tentzeris, "Pattern and frequency reconfigurable annular slot antenna using pin diodes," *IEEE Trans. Antennas Propag.*, Vol. 54, 439–448, Feb. 2006.
17. Yang, S. L. S. and K. M. Luk, "Design of a wide-band L-probe patch antenna for pattern reconfiguration or diversity applications," *IEEE Trans. Antennas Propag.,* Vol. 54, 433–438, Feb. 2006.
18. Mirzavand, R., A. Abdipour, G. Moradi, and M. Movahhedi, "Full-wave semiconductor devices simulation using ADI-FDTD Method," *Progress In Electromagnetics Research M*, Vol. 11, 191–202, 2010.
19. Liu, Y. H., Q. H. Liu, and Z.-P. Nie, "A new efficient FDTD time-to-frequency-domain conversion algorithm," *Progress In Electromagnetics Research*, Vol. 92, 33–46, 2009.
20. Faghihi, F. and H. Heydari, "Time domain physical optics for the higher-order FDTD modeling in electromagnetic scattering from 3-D complex and combined multiple materials objects," *Progress In Electromagnetics Research*, Vol. 95, 87–102, 2009.
21. Zhang, Y.-Q. and D.-B. Ge, "A Unified FDTD approach for electromagnetic analysis of dispersive objects," *Progress In Electromagnetics Research*, Vol. 96, 155–172, 2009.
22. Camp, M., H. Gerth, H. Garbe, and H. Haase, "Predicting the breakdown behavior of microcontrollers under EMP/UWB impact using a statistical analysis," *IEEE Trans. Electromagn. Compat.*,

Vol. 46, No. 3, 368379, Aug. 2004

23. Camp, M. and H. Garbe, "Parameter estimation of double exponential pluses (EMP, UWB) with least squares and ncular mead algorithm," *IEEE Trans. Electromagn. Compat.*, Vol. 46, No. 4, 368379, Aug. 2004
24. Taflove, A. and S. C. Hagness, *Computational Electrodynamics: The Finit-difference Time-domain Method*, 2nd edition, Arthech House, MA, Norwood, 2000.
25. Noda, T. and S. Yokoyama, "Thin wire representation in finite difference time domain surge simulation," *IEEE Trans. Power Del.*, Vol. 17, No. 3, 840–847, Jul. 2002.
26. Umashankar, K. R., A. Taflove, and B. Beker, "Calculation and experimental validation of induced currents on coupled wires in an arbitrary shaped cavity," *IEEE Trans. Antennas Propag.,* Vol. 35, No. 11, 1248–1257, Nov. 1987.
27. Hyun, S. Y., S. Y. Kim, and Y. S. Kim, "An equivalent feed model for the FDTD analysis of antennas driven through a ground plane by coaxial lines," *IEEE Trans. Antennas Propag.,* Vol. 57, No. 1, 161–167, Jan. 2009.
28. Johnk, C. T. A., *Engineering Electromagnetic Fields and Waves*, 2nd edition, 495–501, Wiley, New York, 1988.
29. Lu, J. W., D. Thiel, and S. Saario, "FDTD analysis of dielectric-embedded electronically switched multiple-beam (DE-ESMB) antenna array," *IEEE Trans. Magnetics*, Vol. 38, No. 2, 701–704, Mar. 2002.